Frustration wave order in iron(II) oxide spinels

Giuditta Perversi, Ángel M Arévalo-López, Clemens Ritter, J. Paul Attfield

HAL Id: hal-02297713

https://hal.univ-lille.fr/hal-02297713

Submitted on 5 Jan 2021

Frustration wave order in iron(II) oxide spinels

Giuditta Perversi[1], Angel M. Arevalo-Lopez[1,2], Clemens Ritter[3] & J. Paul Attfield [1]

Frustrated magnetic materials can show unconventional correlations such as quantum spin liquid states and monopole excitations in spin ices. These phenomena are observed on uniformly frustrated lattices such as triangular, kagome or pyrochlore types, where all nearest neighbour interactions are equivalent. Here we report incommensurate long-range spin amplitude waves in the spinels Fe_2GeO_4 and γ-Fe_2SiO_4 at low temperatures, which indicate that the degree of frustration may itself be a fluctuating quantity that can spontaneously order without a lattice distortion as a 'frustration wave'. Fe_2GeO_4 with propagation vector $(\frac{2}{3} + \delta \ \frac{2}{3} + \delta \ 0)$ has ordered Fe^{2+} moments that vary between fully saturated 4 μB and 0 values, consistent with a frustration wave order. γ-Fe_2SiO_4 has a more complex $(\frac{3}{4} + \delta \ \frac{3}{4} + \delta \ 0)$ order that coexists with an ordered spin ice phase. Dynamic orbital fluctuations are proposed to give rise to locally correlated patterns of ferromagnetic and antiferromagnetic interactions consistent with the observed orders.

[1] Centre for Science at Extreme Conditions (CSEC) and School of Chemistry, University of Edinburgh, Mayfield Road, Edinburgh EH9 3JZ, UK. [2] Univ. Lille, CNRS, Centrale Lille, ENSCL, Univ. Artois, UMR 8181 - UCCS - Unité de Catalyse et Chimie du Solide, F-59000 Lille, France. [3] Institute Laue Langevin, BP 15638042 Grenoble, France. Correspondence and requests for materials should be addressed to J.P.A. (email: j.p.attfield@ed.ac.uk)

ong-range spin order is sometimes avoided in frustrated magnetic materials, leading to unconventional correlations such as quantum spin liquids and ices[1–4]. Frustrated long-range spin orders are also observed and the degree of frustration for an individual spin or a larger grouping within the ordered lattice may be quantified by the function:[5]

$$F = \tfrac{1}{2}\left(1 - \sum J_{ij}\mathbf{S}_i.\mathbf{S}_j / \sum |J_{ij}||\mathbf{S}_i||\mathbf{S}_j|\right)$$

where the exchange Hamiltonian for interacting spins $\mathbf{S}_i$ and $\mathbf{S}_j$ is $-J_{ij}\mathbf{S}_i.\mathbf{S}_j$. F varies between 0 for unfrustrated spins and 1 for complete frustration. For a collinear spin order on a simple lattice in which exchange couplings are equivalent and are either fully frustrated or unfrustrated, the degree of frustration simplifies to $F = N_f/N$, where N_f is the number of frustrated interactions and N is the total number of interactions around each spin. Conventional frustrated systems have constant F at all spins, for example, the canonical pyrochlore-type lattice of corner-sharing tetrahedra of antiferromagnetically interacting moments has $F = 1/3$ at all sites in the ordered ground states shown in Fig. 1(a, b). The related '2-in 2-out' spin ice order shown in Fig. 1(c) is also uniformly frustrated. The physics of many investigated pyrochlores is thus predicated on the uniformity of the degree of frustration (F) throughout the lattice.

Fe$_2$GeO$_4$ and the high-pressure γ-form of Fe$_2$SiO$_4$ are cubic B$_2$AO$_4$ spinels, where orbitally degenerate $3d^6$ Fe^{2+} cations with $S = 2$ spins form a pyrochlore-type B-site lattice[6,7]. γ-Fe$_2$SiO$_4$ is also of geophysical interest as one of the main constituents of the Earth's mantle[8,9]. Previous studies have established that both materials have magnetic transitions near 10 K[10–14], but the low-temperature spin orders are not reported and preliminary abstracts have differing results[15,16]. Our investigation of their magnetic structures has led to the discovery of frustration wave order as a class of ground states, where spin–spin interactions become spatially non-uniform within a structurally uniform lattice.

Results

Spin order in Fe$_2$GeO$_4$. Synthesis of the polycrystalline Fe$_2$GeO$_4$ sample and characterisation measurements are described in methods with further details in Supplementary Figs. 1, 5 and 6,

Supplementary Tables 1, 3 and 4 and Supplementary Notes 1 and 2. Magnetic susceptibility measurements (Fig. 2a) for Fe$_2$GeO$_4$ reveal two magnetic transitions with a susceptibility maximum at $T_{m1} \approx 9$ K and divergence of field and zero-field cooled susceptibilities at $T_{m2} \approx 7$ K, consistent with a previous report[12]. Alternating Current (AC) measurements show no frequency dependence in the low-temperature features, indicating an absence of the spin–glass behaviour (Fig. 2b). A broad magnetic contribution to the low-temperature heat capacity appears to extend up to around 50 K (Fig. 2c), but the integrated entropy over the two transitions of 5.77 J mol^{-1} K^{-1} per Fe^{2+} is only 43% of the theoretical value of $R\ln5$ for long-range order of $S = 2$ spins. Fits to synchrotron powder X-ray diffraction data at 5 K, as well as the neutron data below, show that the crystal structure remains cubic $Fd\bar{3}m$ at low temperatures with no distortion observed (Fig. 2d). This is unusual as spin orders in oxide spinels usually lead to lattice distortions, e.g. ZnV$_2$O$_4$[17], LiMn$_2$O$_4$[18], MgCr$_2$O$_4$[19] and Co$_2$GeO$_4$[11,20] all distort from cubic to tetragonal symmetry at orbital or antiferromagnetic ordering transitions. Hence the measurements indicate that the orbital states and a large fraction of the Fe^{2+} spins remain dynamic below the two magnetic transitions.

Sharp magnetic diffraction peaks indicative of long-range spin order appear below the magnetic transition at $T_{m1} \approx 9$ K with an additional weak peak observed below $T_{m2} \approx 7$ K, as shown in Fig. 3a. These peaks were indexed by very similar propagation vectors $\mathbf{k}_i = (2/3 + \delta_i, 2/3 + \delta_i, 0)$ for peaks appearing below T_{mi} ($i = 1$ or 2). Representation analysis shows that the single Fe B lattice position is split into magnetically distinct Fe1 and Fe2 sites. The magnetic intensities from each transition are fitted by a double-k model, in which different propagation vectors $\mathbf{k}_{ij}$ apply to different sites Fej ($j = 1$ or 2), $\mathbf{k}_{i1} = (2/3 + \delta_i, -2/3 - \delta_i, 0)$ and $\mathbf{k}_{i2} = (2/3 + \delta_i, 2/3 + \delta_i, 0)$. A good fit to the peaks that are observed below T_{m1}, as shown in Fig. 3b where refined $\delta_1 \approx -0.025(1)$, can only be obtained using a model in which ordered moment amplitudes are modulated, as displayed in Fig. 3c. The sublattices of Fe1 and Fe2 spins are mutually perpendicular and each has collinear antiferromagnetic chains of spins pointing parallel to their propagation direction. The additional magnetic peak observed below T_{m2} is fitted by an additional order of small perpendicular moment components that describe a canting of the above
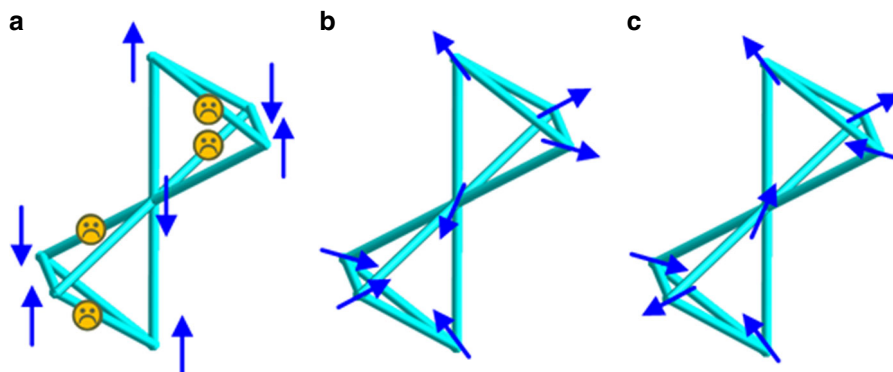

Fig. 1 Frustrated magnetic order on a uniform pyrochlore lattice. Spins lie at the apices of a lattice of corner-sharing tetrahedra, and all nearest-neighbour couplings are of equal magnitude, as represented by the blue lines. **a** A ground-state configuration for collinear spin order when the nearest-neighbour couplings are antiferromagnetic. This ground state is highly degenerate, but lattice distortion may stabilise one configuration. Four antiferromagnetic couplings are satisfied in each tetrahedron and two are frustrated as indicated by 'sad face' symbols; this construct is useful for the more complex frustrated configurations shown in Fig. 4. **b** Non-collinear spin order for situation (**a**) can give rise to the 'all-in all-out' configuration, where all magnetic moments point towards or away from the centre of each B-site tetrahedron, preserving cubic symmetry and with each antiferromagnetic coupling partly frustrated. **c** Strong dipolar interactions can lead to a related '2-in 2-out' spin ice order, with two spins pointing in and two pointing out of each tetrahedron when spin–spin couplings are weakly ferromagnetic. This is also shown as one of the magnetic phases for γ-Fe$_2$SiO$_4$ in Fig. 5e
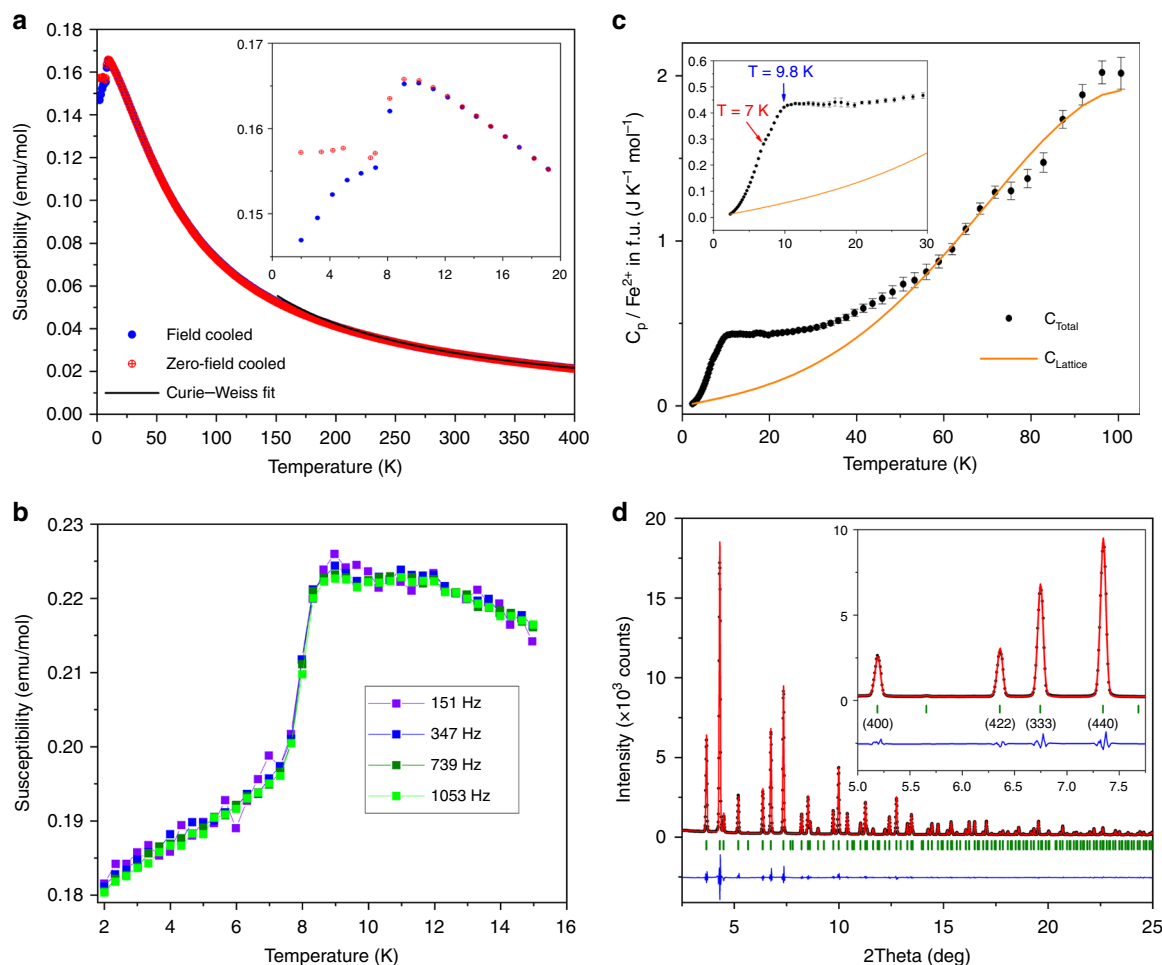
Fig. 2 Magnetic and structural characterisation of Fe_2GeO_4. **a** Magnetic susceptibility in an applied field of 0.5 T with inset is showing the low-temperature region where magnetic transitions occur at $T_{m1} \approx 9$ K and $T_{m2} \approx 7$ K. The Curie–Weiss fit to points between 150 and 400 K gives an effective paramagnetic moment of 4.25 μ_B, consistent with high-spin 3d^6 Fe^{2+} spins and a Weiss temperature of $\theta = -19.6$ K **b** Real part of the AC susceptibility in an oscillating magnetic field with amplitude 9 Oe and frequencies as shown. No frequency dependence of the features that would evidence spin–glass behaviour is observed. **c** Heat capacity variation with the lattice contribution fitted by the polynomial $C_p = \gamma T + \beta T^3 + \delta T^5$. The inset shows the low-temperature region with discontinuities at T_{m1} and T_{m2} marked. The magnetic contribution is evident up to 55 K, but the integrated entropy in the 2–55 K range of 5.77 J mol^{-1}K^{-1} is only 43% of the theoretical $R\ln(2S + 1) = 13.38$ J mol^{-1} for $S = 2$. Error bars are standard deviations. **d** Fit of the cubic spinel model to the synchrotron X-ray diffraction profile ($\lambda = 0.1917$ Å) at 5 K with the region containing (400) and (440) reflections that are sensitive to a tetragonal lattice distortion shown in the inset. No peak splittings or broadenings that would evidence a lattice distortion are observed

magnetic structure. Temperature variations of the moment amplitudes μ_i and propagation vector shifts δ_i are shown in Fig. 3d and the maximum amplitudes of the two modulated moment components are $\mu_1 = 3.94(3)$ and $\mu_2 = 0.92(7)$ μ_B at 1.8 K. The maximum resultant amplitude is $\mu = 4.05(8)$ μ_B, in agreement with the ideal value of 4 μ_B for high-spin Fe^{2+}. Ordered moments are modulated between 0 (fully frustrated) and 4 μ_B (unfrustrated) values. The average ordered moment magnitude is 64% of the ideal value, so the equivalent of approximately one-third of the spins remain dynamic below the magnetic ordering transitions, qualitatively consistent with the substantial reduction of magnetic entropy.

Frustration wave picture for Fe_2GeO_4. Amplitude-modulated spin-density wave (SDW) order of local moments is relatively common in metallic magnets, where exchange couplings are coupled to the Fermi surface vectors, as described in RKKY theory. However, amplitude modulation of moments between zero and fully saturated values as observed in Fe_2GeO_4 is highly

unusual in non-metallic materials, as even complex spin textures such as helimagnets, spin vortices or skyrmions have uniform moment amplitudes, while spin directions change. Elliptical spiral structures in frustrated systems can modulate moment amplitudes over part of the available range, e.g. in $FeTe_2O_5Br$[21], and 'idle spin' orders provide a special case where some spins remain disordered due to frustration of their interactions with surrounding uniformly ordered spins, an example is observed below 0.7 K in the pyrochlore $Gd_2Ti_2O_7$[22]. The only close SDW analogue to Fe_2GeO_4 we are aware of is the spin order in $Ca_3Co_2O_6$[23], where chains of collinear moments are modulated between 0 and 5.0 μ_B moments for $S = 2$ Co^{3+} moments with a sizable orbital contribution.

Strongly frustrated systems based on orbitally non-degenerate ions such as $S = 5/2$ Fe^{3+} in $FeTe_2O_5Br$ and $S = 7/2$ Gd^{3+} in $Gd_2Ti_2O_7$ can stabilise spin arrangements of varying amplitude to minimise exchange energy between unfavourably oriented moments and gain entropy from the thermally fluctuating components at non-zero temperatures. However, the observation
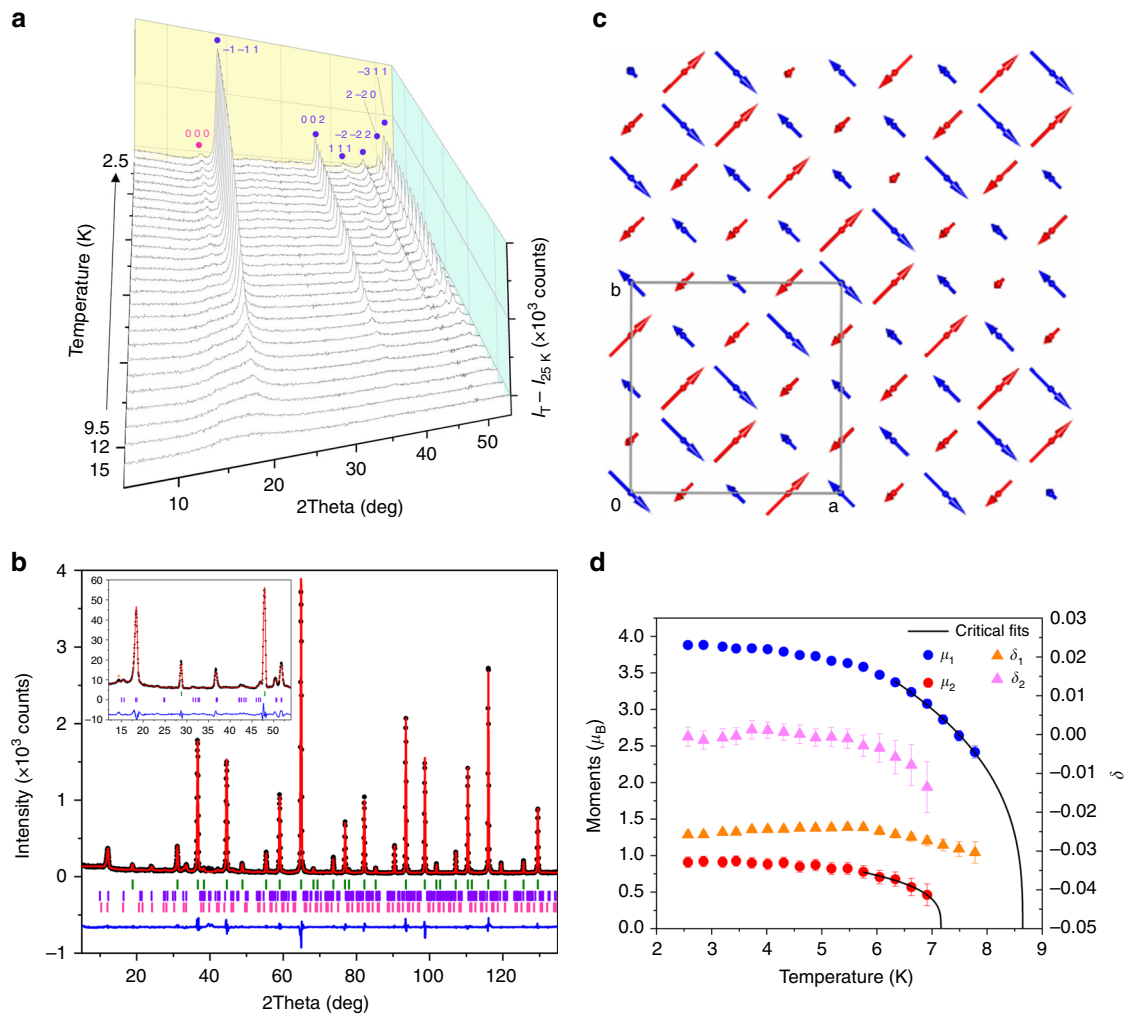
Fig. 3 Low-temperature neutron diffraction results for Fe₂GeO₄. **a** Magnetic scattering profiles obtained by subtracting the 25 K D20 data from profiles between 2.5 and 9.5 K, recorded in ~0.3 K steps and at 12 and 15 K. *h k l* labels correspond to magnetic satellite reflections at $(hkl) + \mathbf{k}_i$ for $\mathbf{k}_i = (^2/_3 + \delta_i \, ^2/_3 + \delta_i \, 0)$. The five magnetic peaks with black labels that appear below $T_{m1} = 8.9$ K have a propagation vector $\mathbf{k}_1$, while the weak 000 peak indicated in pink appears below $T_{m2} = 6.6$ K with vector $\mathbf{k}_2$. **b** Fit of the crystal and magnetic structures at 2 K to high-resolution D2B data at 2 K ($\lambda = 1.59$ Å). The inset shows the fit in the low-angle region of D20 data ($\lambda = 2.41$ Å). Two weak impurity peaks are labelled with asterisks. Magnetic reflection markers are in violet ($\mathbf{k}_1$) and pink ($\mathbf{k}_2$), and the structural reflections are in green. **c** The $\mathbf{k}_1$ order below T_{m1} with sinusoidal modulation of the Fe1 (blue) and Fe2 (red) moment amplitudes in the [1$\bar{1}$0] and [110] directions, respectively. Moments vary between 0 (fully frustrated) and 4 μ_B (fully ordered) values. The additional $\mathbf{k}_2$ order below T_{m2} adds a small modulated tilting of the moments shown separately in Supplementary Fig. 6. **d** Temperature variations of the magnetic moments μ and propagation vector contributions δ for Fe1 and Fe2 with canting in the *ab*-plane. Fits of the critical law $\mu = \mu_0(1 - T/T_m)^\beta$ to the moment variations are shown, where $\beta_1 = 0.35(6)$ and $T_{m1} = 8.6(2)$ K, and $\beta_2 = 0.3(1)$ and $T_{m2} = 7.2(2)$ K for the two transitions. Error bars are standard deviations

of very rare collinearly ordered components with full amplitude modulation to lowest temperature in Fe₂GeO₄ and Ca₃Co₂O₆, both of which are based on high-spin 3d⁶ ions with unquenched orbital contributions, suggests that an additional factor operates in these materials. We propose that dynamic correlations of the orbital and spin states in these materials give rise to modulations of *F* that match the periodicity of the SDW, hence a 'frustration wave'.

The orbital interactions and resulting magnetic exchange interactions that can give rise to frustration wave order in Fe₂GeO₄ are shown in Fig. 4. High-spin Fe²⁺ cations have the degenerate $t_{2g}^4 e_g^2$ ground state with one doubly occupied and two half-occupied t_{2g} orbitals, and t_{2g}–t_{2g} magnetic exchange interactions occur across the shared edges of FeO₆ octahedra, as well as more weakly through the 90° Fe-O-Fe pathway. Only one of the three t_{2g} orbitals on each Fe²⁺ cation overlaps with another in

the 90° Fe-O-Fe pathway, hence three electronic possibilities exist. Direct t_{2g}^1–t_{2g}^1 interactions are antiferromagnetic (J_{AF}), but the t_{2g}^2–t_{2g}^1 interactions are ferromagnetic (J_F), in keeping with Goodenough–Kanamori exchange rules[24,25] or the Kugel–Khomskii approach[26], as shown in Fig. 4a. We assume that coulombically unfavourable t_{2g}^2–t_{2g}^2 configurations are avoided at low temperatures, as observed in the orbitally ordered ground state of magnetite[27]. This corresponds to a local orbital ordering constraint. Each tetrahedron of four Fe²⁺ spins thus has two antiferromagnetic t_{2g}^1–t_{2g}^1 and four ferromagnetic t_{2g}^2–t_{2g}^1 interactions along its edges, and these have two distinct arrangements as shown in Fig. 4b. The configuration where antiferromagnetic couplings are on adjacent (A) edges of the tetrahedron is notable, as the simplest collinear ground state for comparable interaction strengths $J_{AF} \approx -J_F$ is a 3 up/1 down configuration in which two spins are unfrustrated (*F* = 0), while
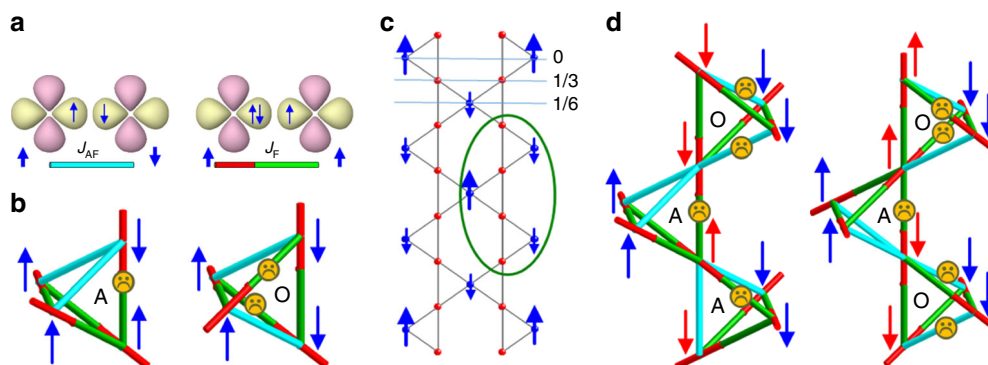
Fig. 4 Frustration wave model for orbital and spin correlations in Fe_2GeO_4. **a** Nearest-neighbour Fe^{2+}–Fe^{2+} t_{2g} orbital and magnetic interactions. The t_{2g}^1–t_{2g}^1 interaction (left) leads to antiferromagnetic coupling J_{AF} between cation spins shown in the lower corners and is represented by the light blue bar below and in (**b**) and (**d**). The t_{2g}^2–t_{2g}^1 interaction (right) shows t_{2g}^2 orbital order and associated ferromagnetic coupling J_F, respectively, represented by red and green bars below and in (**b**) and (**d**). **b** The two configurations for orbital order and magnetic interactions within the tetrahedra of four Fe^{2+} cations. Four edges have orbital order and ferromagnetic couplings and two are antiferromagnetic. Tetrahedra with antiferromagnetic couplings on adjacent (A, left hand image) edges have a 3 up/1 down spin ground state for $J_{AF} \approx -J_F$, where the two spins adjacent to the frustrated interaction are partially frustrated, but the others are unfrustrated. The alternative configuration has antiferromagnetic couplings on opposite (O, right hand image) edges and is uniformly frustrated with ferromagnetic and antiferromagnetic ground states of comparable energy for $J_{AF} \approx -J_F$, the latter is shown here. **c** ($2/3$ $-2/3$ 0) approximant model for the Fe1 spin order in Fe_2GeO_4 shown in Fig. 3c, projected on the [110] plane of the cubic spinel structure. Fe1 moments form ferromagnetic chains perpendicular to the image plane; one-third have fully ordered up spins (Fe1: $+S$) and two-thirds are partially fluctuating down spins (Fe1:$-S/2$). Perpendicular ordered spins at Fe2 sites (red) are not shown. Values of the frustration index F in the different spin layers are shown. **d** Two fluctuating configurations for orbital and spin orders within the representative unit circled in (**c**). Static Fe1 spin components (blue) are coupled through dynamic components of the Fe2 spins (red). The central tetrahedron is always A-type and the two blue (Fe1: $+S$) spins have no frustrated interactions to nearest-neighbours and are fully ordered. The top and bottom tetrahedra fluctuate between A and O configurations and have (Fe1:$-S/2$) spins with some frustrated interactions. Fe2 spin components fluctuate between up and down in these and other configurations and have no static ordered component parallel to Fe1 spins

the other two are partially frustrated ($F = 1/3$). This demonstrates how large variations in F between neighbouring spins may arise as a result of the local orbital ordering configuration. The alternative arrangement with antiferromagnetic couplings on opposite (O) tetrahedral edges has all spins equally frustrated ($F = 1/3$). There are 24 equivalent A-type configurations, but only six for O-types, hence (neglecting any long range orbital correlations) 80% of Fe_4 tetrahedra are A-type at any instant in the orbitally fluctuating state in the absence of longer-range orbital correlations and 16% of Fe^{2+} spins are in a locally unfrustrated ($F = 0$) environment at the apices between two A-type tetrahedra. This shows that dynamically correlated orbital fluctuations (dynamic orbital order) can lead to large local fluctuations in F, and long-range magnetic and frustration wave order at low temperatures.

We propose that frustration wave order in Fe_2GeO_4 arises from exchange interactions between ordered spin components in one sublattice via the dynamic components of their neighbours in the other. This is illustrated using the ordered Fe1 spins, which are represented by a commensurate approximant ($2/3$ $-2/3$ 0) model for simplicity in Fig. 4c (the small incommensurability most likely results from next nearest-neighbour Fe–O...O–Fe magnetic couplings that are neglected here). Ferromagnetic chains of fully ordered Fe1 up spins ($+S$) and partially fluctuating Fe1 down spins with ordered components of $-S/2$ are linked by Fe2 spins that are ordered in a perpendicular direction, so no Heisenberg exchange occurs. However, fluctuating components of Fe2 spins can couple to Fe1 spins as shown in Fig. 4d. The observed order is consistent with A-type tetrahedra leading to unfrustrated interactions around the Fe1 ($+S$) chain, while other tetrahedra fluctuate between A and O configurations leading to some frustrated interactions at the other Fe1 ($-S/2$) chains. The Fe2 spin components fluctuate between up and down states in the

various configurations and have no static order parallel to Fe1 spins. The orbital states fluctuate in a highly correlated manner but without leading to localisation and orbital order. Similar orbital pictures can be drawn for any sampled region in the full incommensurate structure (Fig. 3c). The modulation of the F consistent with the commensurate approximant ($2/3$ $-2/3$ 0) model for Fe_2GeO_4 is shown in Fig. 4c. The Fe1 ($+S$) spins are always unfrustrated while those at Fe2 sites are highly frustrated with pyrochlore-like $F = 1/3$ values, and the partly frustrated Fe1 ($-S/2$) spins have intermediate values, shown as $F = 1/6$ on the assumption of equal fluctuations between A and O configurations of their local spin tetrahedra.

Spin Order in γ-Fe_2SiO_4. The high-pressure spinel γ-Fe_2SiO_4 was also studied to investigate the chemical pressure effects of replacing Ge in Fe_2GeO_4 by smaller Si. High-pressure synthesis of the polycrystalline γ-Fe_2SiO_4 sample and characterisation measurements are described in methods with further details in Supplementary Figs. 2, 3, 4 and 7, Supplementary Tables 2, 5, 6 and 7 and Supplementary Notes 1 and 3. Two magnetic ordering transitions are observed in low-temperature neutron diffraction profiles of γ-Fe_2SiO_4, as shown in Fig. 5a and b. Magnetic diffraction peaks appearing below $T_{m1} = 12$ K are indexed by propagation vector $\mathbf{k}_1 = (3/4 + \delta_1$ $3/4 + \delta_1$ 0), where $\delta_1 \approx 0.030(1)$, and are fitted by double-k magnetic structures, similar to that of $\mathbf{k}_1$-Fe_2GeO_4. Two modulated spin components are present and their combinations can describe a canted arrangement (Fig. 5c) or an elliptical helical order (Fig. 5d). These fit the magnetic intensities equally well, and the ordered moment amplitudes are modulated in both cases, so it is not clear whether this is a frustration wave or a more conventional elliptical spin order.
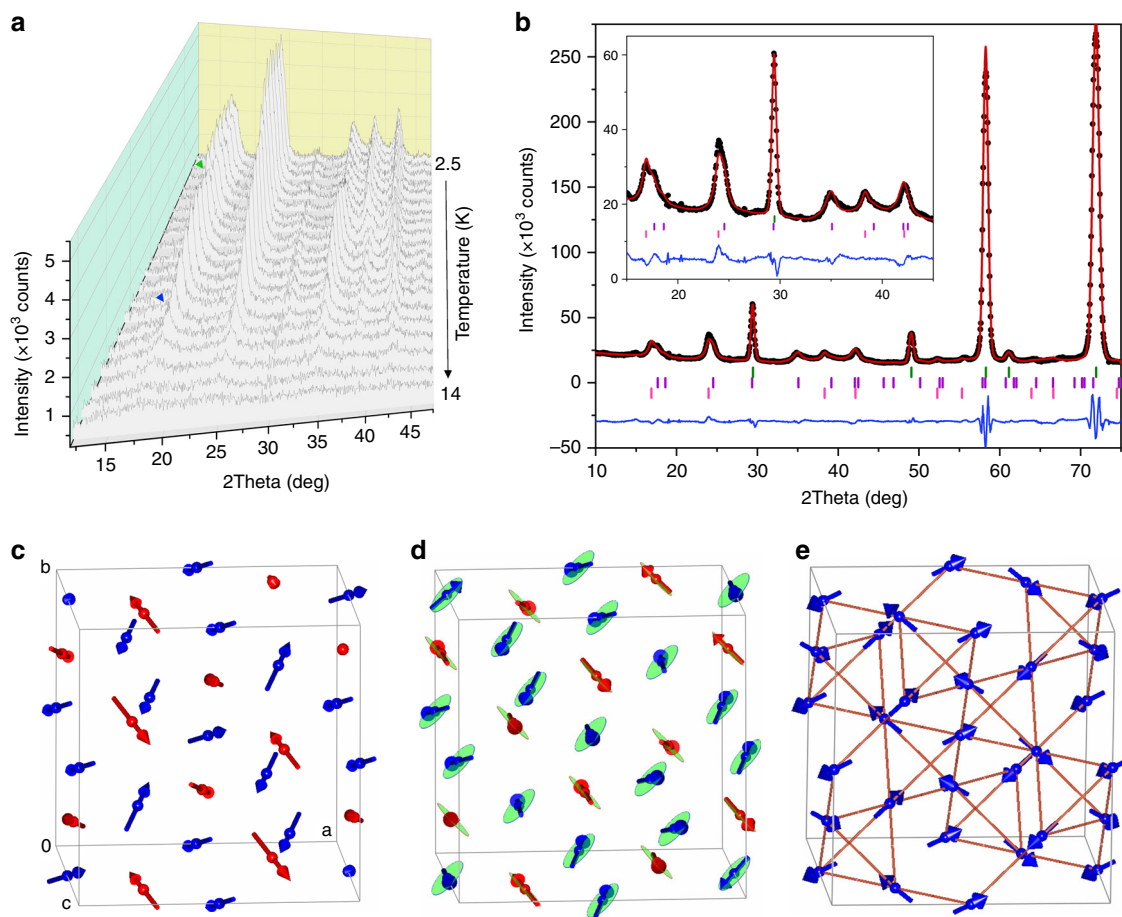
Fig. 5 Low-temperature neutron diffraction results for γ-Fe_2SiO_4. **a** Magnetic scattering profiles obtained by subtracting 25 K D20 data from profiles between 2.5 and 14 K, increasing in ~0.6 K steps. Blue and green arrows, respectively, show changes in diffraction intensity at the $T_{m1} = 13$ K and $T_{m2} = 8$ K transitions. **b** Fit of the crystal and magnetic structures at 2 K to D20 data at 2 K with 90° takeoff angle. The inset shows the fit to prominent magnetic peaks in the low-angle region for data with 42° takeoff angle to give high resolution. Magnetic reflection markers are in violet (k_1) and pink (k_2), and structural reflections are in green. **c** Canted model for the $k_1 = (3/4 + δ\ 3/4 + δ\ 0)$ order is observed below T_{m1}, showing Fe1 (blue) and Fe2 (red) moments. (**d**) Alternative elliptical helix model for the k_1 order is showing the planes of rotation for the moments. (**e**) The additional $k_2 = (1\ 0\ 0)$ ordered spin ice phase is observed below T_{m2}, showing the tetrahedra of 2-in-2-out moments

Further magnetic peaks that emerge below $T_{m2} = 8$ K for γ-Fe_2SiO_4 are indexed on a commensurate $k_2 = (1\ 0\ 0)$ vector and are fitted by an ordered spin ice model (Fig. 1c, 5e), in which all moment amplitudes are equal. Spin ice ordering is very rare in transition metal oxide spinels, but is reported in the V^{3+} sublattice of FeV_2O_4, although this phase is tetragonally distorted with both Fe^{2+}–V^{3+} and V^{3+}–V^{3+} magnetic interactions operating[28]. The observation of a spin ice phase competing with the modulated wave state reveals a fine energy balance between these two classes of ground state in γ-Fe_2SiO_4. Long-range spin ice orders in pyrochlore oxides such as $Sm_2Mo_2O_7$ and $Nd_2Mo_2O_7$ result from weak exchange coupling and large dipolar interactions coupled with local anisotropy[29]. Local variations of ferromagnetic and antiferromagnetic couplings driven by the correlated orbital fluctuations may also help to stabilise the spin ice phase of γ-Fe_2SiO_4.

moment in the magnetically ordered phases. This arises because the exchange interactions depend on the d-orbital occupancy, so that a coupling of spins and orbitals can give rise to a long-range modulation of the exchange interactions and hence the frustration function. Weak coupling of Fe^{2+} orbital states to the lattice appears to be important for avoiding structural distortions that probably destabilise frustration wave orders in other orbitally degenerate materials. The γ-Fe_2SiO_4 analogue has a more complex modulated order that may be frustration wave driven, competing with a spin ice phase. Frustration waves lead to spatial organisation of statically ordered and highly correlated, but dynamic orbital and spin components that may give rise to novel excitations and quantum phenomena in these and other materials. Further exploration of the complex spin orders in Fe_2GeO_4 and γ-Fe_2SiO_4 using single crystals and of their excitations by inelastic neutron scattering and other spectroscopies will thus be worthwhile.

Discussion

In conclusion, the unusual magnetic structure of Fe_2GeO_4 evidences a previously unrecognised class of ground states for orbitally degenerate spins on frustrated lattices, in which the degree of frustration orders spatially across structurally equivalent sites, resulting in large amplitude modulations of the

Methods

Sample synthesis and characterisation. Fe_2GeO_4 and olivine-type α-Fe_2SiO_4 were synthesised as polycrystalline powders by grinding stoichiometric quantities of Fe (-22 mesh, 99.998%, Alfa Aesar), GeO_2 / SiO_2 (99.999% Alfa Aesar) and Fe_2O_3 (99.999% Sigma Aldrich) powders and pressing them into a pellet. The reactions were carried out in evacuated silica tubes, heating in a

box furnace at 900 °C for 60 h and then slow-cooling for 12 h. α-Fe$_2$SiO$_4$ was transformed to spinel-type γ-Fe$_2$SiO$_4$ in a Walker-type multi-anvil press in BN capsule, pressurising at 6 GPa at 900 °C for 20 min before quenching. Laboratory X-ray diffraction using a Bruker D2 diffractometer confirmed the formation of cubic $Fd\overline{3}m$ normal spinels with Fe^{2+} only at the octahedral B-sites. Physical measurements were performed using a Quantum Design MPMS XL7 SQUID magnetometer for DC susceptibility and a Quantum Design PPMS for AC susceptibility and heat capacity measurements.

Powder neutron diffraction. Powder neutron diffraction (PND) data were collected at the ILL facility in Grenoble. High-resolution profiles for a 3 g sample of Fe$_2$GeO$_4$ were collected on instrument D2B at wavelength λ = 1.59475 Å with 10' collimation at 2 K and at full flux at 2, 6, 10, 50, 100, 200 and 300 K. Refinements were performed on high-resolution integrated data from the central region of the detector. Additional PND data were collected from D20 with λ = 2.41 Å at 1.8, 2.5, 12, 15 and 25 K; ramp collection between 2.5 and 9.5 K in ~ 0.3 K steps was used to follow the evolution of the magnetic structure. PND data for γ-Fe$_2$SiO$_4$ were collected between 2 and 300 K from D20 (λ = 2.41) on 120 mg sample. Data acquired with high takeoff angle (90°) were used for crystal structure refinement to confirm cubic symmetry, whereas low takeoff angle (42°) data were used for magnetic structure determination.

The structural and magnetic refinements were performed with the Rietveld refinement routines implemented in FullProf, using the k-search and the BasIreps software for magnetic symmetry determination and analyses[30,31]. Crystal and magnetic structures were visualised with FPStudio in the FullProf suite and with the VESTA software[32]. Representation analysis shows that the single Fe B lattice site is split into magnetically distinct sites, Fe1 at (½,½,½) and Fe2 at (¾,0,¼). Details on the representation analysis and the basis vectors can be found in Supplementary Notes 2 and 3.

Magnetic diffraction peaks appearing below the two Fe$_2$GeO$_4$ transitions have very similar propagation vectors $\mathbf{k}_i = (^2/_3 + \delta_i\ ^2/_3 + \delta_i\ 0)$. The first order is incommensurate with $\delta_1 \approx$ -0.025(1), but assuming that $\delta_1 = \delta_2$ does not fit the peak positions for the second phase correctly and refining the propagation vector shift independently gives $\delta_2 \approx 0$. Hence this order appears to be commensurate with vector $\mathbf{k}_2 = (^2/_3\ ^2/_3\ 0)$ as reported elsewhere[15], but observation of more peaks will be needed to confirm its nature. The $\mathbf{k}_2$ spin components are perpendicular to the $\mathbf{k}_1$ moments shown in Fig. 3c, but modelling these in the xy–plane or z-direction gave equally good fits.

γ-Fe$_2$SiO$_4$ has two quite different magnetic phases. The $\mathbf{k}_1 = (^3/_4 + \delta_1\ ^3/_4 + \delta_1\ 0)$ phase appearing below $T_{m1} = 12$ K is similar to that of $\mathbf{k}_1$-Fe$_2$GeO$_4$, but has two amplitude-modulated spin components. Magnetic peaks that emerge below $T_{m2} = 8$ K are indexed on a commensurate $\mathbf{k}_2 = (1\ 0\ 0)$ vector and the intensities are fitted by the ordered spin ice model, showing that this is a separate magnetic phase. Absolute values of the moments cannot be determined without knowledge of the magnetic phase proportions. The maximum amplitude in the canted description of the incommensurate phase with vector $\mathbf{k}_1$ of 2.77(9) μ$_B$ and the 1.29(4) μ$_B$ moment from the spin ice phase with $\mathbf{k}_2$ sum to 4.1(1) μ$_B$ at 1.8 K, indicating that the sample comprises 68% of the $\mathbf{k}_1$ and 32% $\mathbf{k}_2$ phase, both with ideal (maximum) moment values of 4.0 μ$_B$. Moment magnitudes vary between 0 and 4.0 μ$_B$ in the canted model and between 1.8 and 3.6 μ$_B$ for the elliptical helical model for the $\mathbf{k}_1$ phase.

Data availability

Data that support the findings of this study have been deposited at https://doi.org/10.7488/ds/2439.

References

1. Savary, L. & Balents, L. Quantum spin liquids: a review. *Rep. Prog. Phys.* **80**, 016502 (2016).

2. Gingras, M. J. & McClarty, P. A. Quantum spin ice: a search for gapless quantum spin liquids in pyrochlore magnets. *Rep. Prog. Phys.* **77**, 056501 (2014).

3. Castelnovo, C., Moessner, R. & Sondhi, S. L. Magnetic monopoles in spin ice. *Nature* **451**, 42–45 (2008).

4. Starykh, O. A. Unusual ordered phases of highly frustrated magnets: a review. *Rep. Prog. Phys.* **78**, 052502 (2015).

5. Lacorre, P. The constraint functions: an attempt to evaluate the constraint rate inside structures that undergo ordered magnetic frustration. *J. Phys. C: Solid State Phys.* **20**, L775–L781 (1987).

6. Strobel, P., Koffyberg, F. P. & Wold, A. Electrical and optical properties of high-purity p-type single crystals of GeFe$_2$O$_4$. *J. Solid State Chem.* **31**, 209–216 (1980).

7. Welch, M. D., Cooper, M. A. & Hawthorne, F. C. The crystal structure of brunogeierite, Fe$_2$GeO$_4$ spinel. *Mineral. Mag.* **65**, 441–444 (2001).

8. Ringwood, A. E. The constitution of the mantle—II: further data on the olivine-spinel transition Geochim. *Cosmochim. Ac* **15**, 18–29 (1958).

9. Navrotsky, A. & Hughes, L. Thermodynamic relations among olivine, spinel, and phenacite structures in silicates and germanates. V. The system MgO-FeO-GeO$_2$. *J. Solid State Chem.* **16**, 185–188 (1976).

10. Blasse, G. & Fast, J. F. Néel temperatures of some antiferromagnetic oxides with spinel structure. *Philips Res. Rep.* **18**, 393–399 (1963).

11. Vandenberghe, R. E., & De Grave, E. Mössbauer effect studies of oxidic spinels. In *Mössbauer spectroscopy applied to inorganic chemistry*. Long, G.J, Grandjean, F. (Eds.), Springer US (1989).

12. Barton, P. T. et al. Structural distortion below the Néel temperature in spinel GeCo$_2$O$_4$. *Phys. Rev. B* **90**, 064105 (2014).

13. Yong, W., Dachs, E., Withers, A. C. & Essene, E. J. Heat capacity of γ-Fe$_2$SiO$_4$ between 5 and 303K and derived thermodynamic properties. *Phys. Chem. Miner.* **34**, 121–127 (2007).

14. Derzsi, M. et al. Comparative ab initio study of lattice dynamics and thermodynamics of Fe$_2$SiO$_4$- and Mg$_2$SiO$_4$-spinels. *J. Phys. Condens. Mat.* **23**, 105401 (2011).

15. Chaix, L. et al. Frustration induced complex phase diagram in the spinel GeFe$_2$O$_4$. *Poster abstract P.088, ICNS.* http://www.icns2013.org/IOP/media/uploaded/EVIOP/event_192/A%20-%20Magnetic%20oxides.pdf (2013).

16. Zou, T. et al. Spin glass behavior and field induced anisotropic magnetic ordering in S = 2 frustrated spinel. *Abstract K5.009, APS March Meeting.* http://absimage.aps.org/image/MAR16/MWS_MAR16-2015-006763.pdf (2016).

17. Reehuis, M., Krimmel, A., Büttgen, N., Loidl, A. & Prokofiev, A. Crystallographic and magnetic structure of ZnV$_2$O$_4$. *Eur. Phys. J. B* **35**, 311–316 (2003).

18. Wills, A. S., Raju, N. P. & Greedan, J. E. Low-temperature structure and magnetic properties of the spinel LiMn$_2$O$_4$: a frustrated antiferromagnet and cathode material. *Chem. Mater.* **11**, 1510–1518 (1999).

19. Ortega-San-Martin, L., Williams, A. J., Gordon, C. D., Klemme, S. & Attfield, J. P. Low temperature neutron diffraction study of MgCr$_2$O$_4$ spinel. *J. Phys. Condens. Mat.* **20**, 104238 (2008).

20. Diaz, S. et al. Magnetic frustration in the spinel compounds GeCo$_2$O$_4$ and GeNi$_2$O$_4$. *Phys. Rev. B* **74**, 092404 (2006).

21. Pregelj, Zorko et al. Persistent spin dynamics intrinsic to amplitude-modulated long-range magnetic order. *Phys. Rev. Lett.* **109**, 227202 (2012).

22. Stewart, J. R., Ehlers, G., Wills, A. S., Bramwell, S. T. & Gardner, J. S. Phase transitions, partial disorder and multi-k structures in Gd$_2$Ti$_2$O$_7$. *J. Phys. Condens. Mat.* **16**, L321–L326 (2004).

23. Agrestini, S. et al. Nature of the magnetic order in Ca$_3$Co$_2$O$_6$. *Phys. Rev. Lett.* **101**, 097207 (2008).

24. Kanamori, J. Superexchange interaction and symmetry properties of electron orbitals. *J. Phys. Chem. Solids* **10**, 87–98 (1959).

25. Goodenough, J. B. Theory of the role of covalence in the perovskite-type manganites [La, M(II)]MnO3. *Phys. Rev.* **100**, 564–573 (1955).

26. Kugel, K. I. & Khomskii, D. I. The Jahn-Teller effect and magnetism: transition metal compounds. *Sov. Phys. Usp.* **25**, 231–256 (1982).

27. Senn, M. S., Wright, J. P. & Attfield, J. P. Charge order and three-site distortions in the Verwey structure of magnetite. *Nature* **481**, 173–176 (2012).

28. MacDougall, G. J., Garlea, V. O., Aczel, A. A., Zhou, H. D. & Nagler, S. E. Magnetic order and ice rules in the multiferroic spinel FeV$_2$O$_4$. *Phys. Rev. B* **86**, 060414 (2012).

29. Gardner, J. S., Gingras, M. J. & Greedan, J. E. Magnetic pyrochlore oxides. *Rev. Mod. Phys.* **82**, 53–107 (2010).

30. Rodríguez-Carvajal, J. Recent advances in magnetic structure determination by neutron powder diffraction. *Phys. B* **192**, 55–69 (1993).

31. Rodríguez-Carvajal, J. Magnetic structure determination from powder diffraction using the program FullProf. In *Proc. XVIII Conf. Appl. Crystallography* (eds Morawiec, H. & Stróz, D.) Singapore, (World Scientific, 2001).

32. Koichi, M. & Izumi, F. VESTA: a three-dimensional visualization system for electronic and structural analysis. *J. Appl. Crystallogr.* **41**, 653–658 (2008).

Acknowledgements

Author contributions

G.P. and J.P.A. designed the concept for this study. G.P., A.M.A.-L. and C.R. performed the experimental work and data analysis. G.P. and J.P.A. wrote the manuscript with inputs from all authors.

Additional information

Competing interests: The authors declare no competing interests.

Publisher's note: Springer Nature remains neutral with regard to jurisdictional claims in published maps and institutional affiliations.